The University of Osaka
Institutional Knowledge Archive

Title	Temperature lag with the onset of exchange bias, superparamagnetic blocking, and antiferromagnetic ordering in ultrathin ferromagnet/antiferromagnet thin film
Author(s)	Shiratsuchi, Yu; Tao, Yiran; Tsutsumi, Rou et al.
Citation	Journal of Applied Physics. 2021, 130(19), p. 193902
Version Type	VoR
URL	https://hdl.handle.net/11094/89957
rights	This article may be downloaded for personal use only. Any other use requires prior permission of the author and AIP Publishing. This article appeared in Yu Shiratsuchi, Yiran Tao, Rou Tsutsumi, Kentaro Toyoki, and Ryoichi Nakatani, Journal of Applied Physics 130, 193902 (2021) and may be found at https://doi.org/10.1063/5.0060606.
Note	

Temperature lag with the onset of exchange bias, superparamagnetic blocking, and antiferromagnetic ordering in ultrathin ferromagnet/antiferromagnet thin film

Yu Shiratsuchi, Yiran Tao, Rou Tsutsumi, et al.

View Online   **Export Citation**   **CrossMark**

ARTICLES YOU MAY BE INTERESTED IN

Temperature lag with the onset of exchange bias, superparamagnetic blocking, and antiferromagnetic ordering in ultrathin ferromagnet/antiferromagnet thin film

Yu Shiratsuchi,[1,2,a)] (iD) Yiran Tao,[1] Rou Tsutsumi,[1] Kentaro Toyoki,[1] (iD) and Ryoichi Nakatani[1,2] (iD)

AFFILIATIONS

[1]Department of Materials Science and Engineering, Graduate School of Engineering, Osaka University, 2-1 Yamadaoka, Suita, Osaka 565-0871, Japan
[2]Center for Spintronic Research Network, Graduate School of Engineering Science, 1-3, Machikaneyama, Toyonaka 560-8351, Japan

[a)]Author to whom correspondence should be addressed: shiratsuchi@mat.eng.osaka-u.ac.jp

ABSTRACT

The magnetization of a nanosized magnet, such as an ultrathin film, thermally fluctuates and can become superparamagnetic. In ferromagnetic/antiferromagnetic thin films, superparamagnetism can be suppressed in accordance with antiferromagnetic ordering. The exchange bias can also be induced at the ferromagnetic/antiferromagnetic interface, and it is nontrivial whether the superparamagnetic blocking temperature (T_{B_SPM}) can match either the onset temperature of the exchange bias (T_{B_EB}) or the Néel temperature (T_N). In this study, we investigated the temperature dependence of parameters such as coercivity, exchange bias field, magneto-optic Kerr rotation (θ_K), and AC magnetization (M_{AC}) to elucidate the matching of T_{B_EB}, T_{B_SPM}, and T_N in a Pt/Co/Au/Cr$_2$O$_3$/Pt thin film. Based on the temperature dependences of M_{AC}, T_{B_SPM} was yielded as about 283 K. T_{B_EB} and T_N, which were determined based on the temperature dependence of θ_K, were 278 and 282 K, respectively. T_{B_SPM} was almost equal to T_N but T_{B_EB} was smaller. This temperature lag was caused by the difference in the magnetic anisotropy energy required to induce the exchange bias and suppress superparamagnetism.

I. INTRODUCTION

Various strategies have been developed to control the magnetic states of ultrathin films.[1,2] Superparamagnetism is observed when the energy barrier for magnetization reversal is comparable to the thermal energy, that is, $k_B T$ (where k_B is the Boltzmann constant T is the absolute temperature); and therefore, the net magnetization becomes zero when the magnetic field is removed. Superparamagnetism occurs in nanosized magnets, such as nanoparticles (NPs)[3,4] and ultrathin films,[5,6] and is considered to be a problem that limits the manufacture and application of magnetic storage or memory devices. This problem can be resolved by enhancing the effective magnetic anisotropy energy density. A simple method for achieving this is to use magnetic materials with high magnetic anisotropy energy, such as $L1_0$-FePt[7,8] and

$L1_0$-CoPt.[9] Another approach is to utilize the interfacial magnetic anisotropy. A ferromagnetic (FM)/antiferromagnetic (AFM) interface is an interface that enhances the effective magnetic anisotropy energy density (K_{eff}) of the system. For example, 4-nm-diameter Co$_{core}$–CoO$_{shell}$ NPs can suppress superparamagnetism when embedded in an AFM CoO matrix, whereas similar NPs embedded in a non-magnetic Al$_2$O$_3$ matrix are superparamagnetic above 10 K.[10] In this approach, the enhancement of K_{eff} and/or the effective magnetic volume is due to AFM ordering. Hence, in principle, the superparamagnetic blocking temperature (T_{B_SPM}) can match the Néel temperature (T_N) of CoO. In addition to the NP system, the enhancement of K_{eff} because of AFM ordering was also observed in the stacked structure, such as Co/Cr$_2$O$_3$,[11] Co/α-V$_2$O$_3$,[12] and Ni/α-V$_2$O$_3$.[13]

The FM/AFM interfacial magnetic anisotropy also induces an exchange bias, which is a shift of the magnetization curve along the field axis.[14] As a first approximation, the exchange bias field (H_{EB}) is assumed to be maintained up to T_N,[15,16] when the magnetic anisotropy energy of the AFM layer overcomes both the interfacial exchange coupling and thermal agitation. Even in this case, the enhancement in coercivity (H_C), which is another effect of the exchange anisotropy and is accompanied by the disappearance of H_{EB}, persists in the high-temperature regime. To precisely investigate the influence of AFM ordering on superparamagnetic blocking and the appearance of exchange bias, it is necessary to compare T_N, T_{B_SPM}, and the starting temperature of H_C enhancement. However, the precise determination of the starting temperature of the H_C enhancement is difficult because the H_C of the FM layer inherently depends on the temperature but it would be possible by using the superparamagnetic blocking phenomenon.

In this study, we investigated the influence of AFM ordering on T_{B_SPM} and the onset temperature of the exchange bias (T_{B_EB}) using the FM ultrathin film grown on the AFM Cr_2O_3 layer. The FM/Cr_2O_3 interface induces electrically controllable exchange anisotropy based on the magneto-electric (ME) effect,[17,18] which is promising for designing next-generation spintronic/magnetic devices. Moreover, the induced magnetic anisotropy at the FM/Cr_2O_3 (0001) interface is oriented perpendicularly to the film plane,[11,19] which also makes this effect more prominent. Perpendicular magnetic anisotropy (PMA) is also useful for our investigation because of the minimization of the magnetic easy direction dispersion. Our investigation is mainly based on the temperature dependence of H_C, H_{EB}, magneto-optic Kerr rotation angle (θ_K), and temperature dependence of AC magnetization. We discuss the change in the magnetic state with temperature, that is, we verify whether T_{B_SPM} and T_{B_EB} of the ultrathin Co film match T_N, which has been phenomenologically assumed.[15,16,20] This assumption is made partly owing to the difficulty in determining T_N. In this study, we estimated T_N using the magneto-optic Kerr spectrum, which is influenced by optical interference in an AFM Cr_2O_3 thin film. We found that there was a temperature lag for T_{B_SPM} and T_{B_EB}; and the former was almost the same as T_N but the latter was lower. The term "blocking temperature" is typically used in conjunction with superparamagnetism and exchange bias. To avoid confusion, we denote the superparamagnetic blocking temperature by T_{B_SPM}. For the exchange bias, we denote the onset temperature of the exchange bias by T_{B_EB}.

II. EXPERIMENTAL

A Pt (2 nm)/Co (0.25 nm)/Au (1.0 nm)/Cr_2O_3 (30 nm)/Pt (20 nm) thin film was used as the sample. The film was prepared on an α-Al_2O_3 (0001) single-crystalline substrate using an ultrahigh vacuum (UHV) DC magnetron sputtering system with a base pressure less than 1×10^{-6} Pa. The substrate was ultrasonically cleaned using acetone, pure water, isopropanol, and ethanol. A 20-nm-thick Pt buffer layer was deposited directly onto the substrate at 873 K. Subsequently, a Cr_2O_3 layer was deposited onto the buffer layer at 773 K by a reactive sputtering method using an Ar and O_2 gas mixture. Au, Co, and Pt capping layers were subsequently deposited at room temperature. An Au spacer layer was inserted between the FM

Co and AFM Cr_2O_3 layers to tune the interfacial exchange coupling such that the exchange bias persisted up to the high-temperature regime close to T_N.[21] Details of the preparation method, including the sputtering conditions, can be found in Refs. 21 and 22.

After depositing each layer, the surface state was checked using reflection high-energy electron diffraction (RHEED). The RHEED observations were performed in a different UHV chamber connected to the sputtering chamber. The chambers were connected through a gate valve such that the sample was transferred without exposure to air. The RHEED patterns were obtained at an acceleration voltage of 25 kV and a filament current of 50 μA. Figure 1 shows the RHEED images of each layer with [$11\bar{2}0$] (top column) and [$1\bar{1}00$] (bottom column) azimuths of the substrate. Streak diffraction patterns were observed for the Pt buffer layer and Cr_2O_3 layer, which exhibited a well-crystallized flat surface. The spacing of the streaks was different for the orthogonal azimuth, which indicates that the in-plane crystalline orientation was also aligned. By comparing the reciprocal lattice pattern, the diffraction patterns were deduced to be twinned fcc (111) and twinned corundum (0001) for the Pt buffer layer and the Cr_2O_3 layer, respectively. The twin boundaries were along the [$11\bar{2}$] direction of Pt (111) and the [$11\bar{2}0$] direction of Cr_2O_3 (0001). The RHEED patterns for Au and Co were ring shapes superimposed with weak spots. The weak spot patterns changed with the electron azimuth. These RHEED patterns indicate that the Au and Co layers were globally polycrystalline with partially aligned fcc (111) grains. The RHEED patterns of the Pt capping layer were similar to those of the Pt buffer layer, except for the broadening of the streaks. These crystalline orientations are consistent with those observed in Ref. 22.

The magnetic properties were characterized mainly by AC magnetization and magneto-optic Kerr effect (MOKE) magnetometry. The temperature dependence of the AC magnetization was measured to investigate T_{B_SPM} using a quantum design physical property measurement system. AC magnetization measurements were performed at 220–330 K. An excitation magnetic field, with an amplitude of 1 mT, was applied perpendicular to the film plane. The frequency of the excitation field was varied from 300 Hz to 10 kHz. MOKE measurements were performed for polar (P-MOKE) and longitudinal (L-MOKE) configurations. In the polar and longitudinal configurations, a magnetic field was applied perpendicular and parallel to the film plane, respectively. For each configuration, the incidence angles were 10° and 30° from the surface normal. The wavelength of the incident light (λ) was varied from 400 to 850 nm for P-MOKE and was fixed at 670 nm for L-MOKE. The P-MOKE was measured using a JASCO K-250 MOKE measurement system with a cryostat (Oxford Instruments, OptistatCF). This system was equipped with a grating monochromator, and λ can be varied. The MOKE signal was detected by mechanically oscillating the analyzer at a frequency f_{ana}. The analyzer was mounted in front of the photomultiplier and the analyzer rotated with θ such that the $2f_{ana}$ signal became zero with the help of the feedback circuit. Here, θ corresponds to the Kerr rotation angle, θ_K. The temperature dependences of H_{EB}, H_C, and θ_K were determined based on P-MOKE over the temperature range of 265–320 K, unless otherwise specified. For the temperature dependence measurements, the sample was cooled at a magnetic field of $\mu_0 H = +400$ mT.
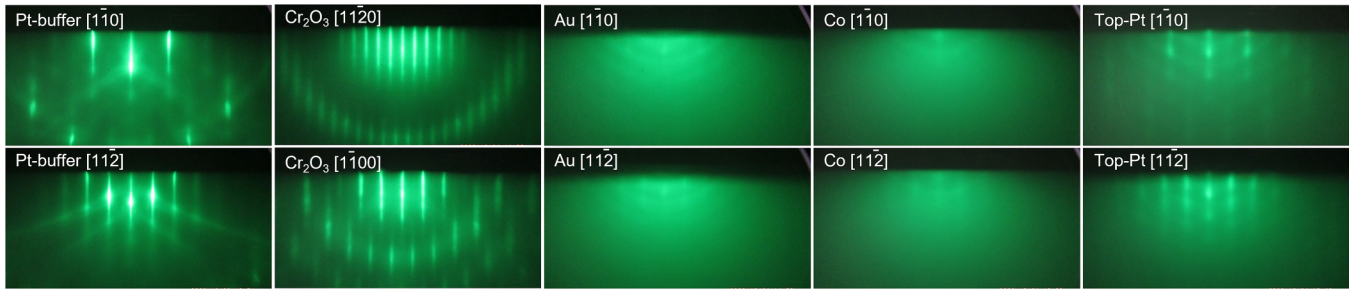
FIG. 1. RHEED images of each layer in the Pt/Co/Au/Cr$_2$O$_3$/Pt thin film. Top and bottom columns correspond to the images with [11$\bar{2}$0] and [1$\bar{1}$00] azimuths of the substrate, respectively.

The anomalous Hall effect (AHE) loops were also measured in the temperature range of 270–320 K with the highest magnetic field of $\mu_0 H = 2$ T, which was applied perpendicular to the film. For the AHE measurements, the film was patterned into a Hall device with a width of 10 μm and length of 50 μm, using photolithography and Ar-ion milling. The AHE results are shown in the Appendix.

III. RESULTS AND DISCUSSIONS

Figure 2 shows the MOKE loops measured at room temperature (~297 K). Both L- and P-MOKE loops exhibited nonlinear curves with zero H_C and zero remanence. θ_K did not saturate at $\mu_0 H = 1.2$ T. This is a typical feature observed when a magnet becomes superparamagnetic. As observed in Fig. 2, the in-plane and out-of-plane magnetization curves (L- and P-MOKE loops)
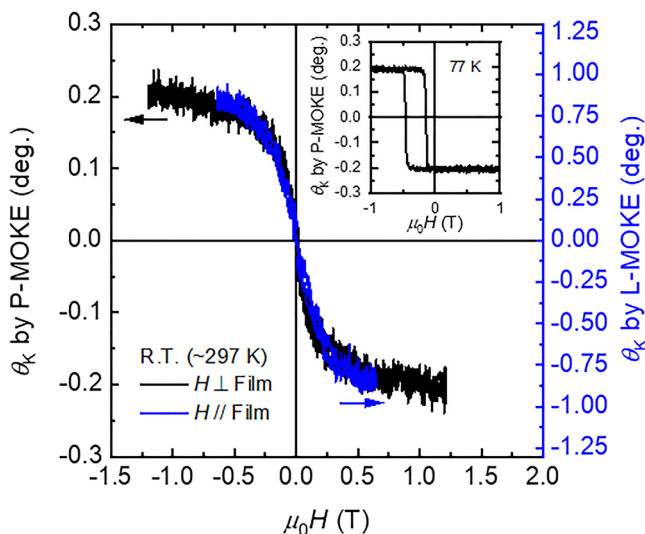

FIG. 2. MOKE loops measured at room temperature (~297 K). Black (left axis) and blue (right axis) curves correspond to the P- and L-MOKE loops for which the magnetic field was applied perpendicular and parallel to the film, respectively. The inset shows the P-MOKE loops measured at 77 K after field cooling.

were similar, and it is difficult to determine the magnetic easy direction at room temperature. The P-MOKE loop measured at 77 K (the inset of Fig. 2) showed rectangular hysteresis, which indicates that the film exhibited PMA. Moreover, $\mu_0 H_{EB}$ of ~420 mT was also measured at 77 K. The appearance of the exchange bias indicates the occurrence of AFM ordering in the Cr$_2$O$_3$ layer, and a high H_{EB} suggests that the interfacial AFM moments were oriented perpendicular to the film plane, as predicted from the spin configuration in the ⟨0001⟩-oriented Cr$_2$O$_3$ layer.[23] In Secs. III A–III C, a magnetic field was applied perpendicular to the film plane and T_{B_SPM}, T_{B_EB}, and T_N were determined to finally compare the obtained values.

A. Determination of T_{B_SPM}

T_{B_SPM} was determined based on the temperature dependence of the AC magnetization, as shown in Fig. 3(a). The in-phase signal (real part) of the AC magnetization (m') showed a peak at 283 K. In the case of the superparamagnetic blocking phenomenon, the out-of-phase signal (imaginary part) of the AC magnetization (m'') can also show a peak in the slightly low-temperature regime. We could not observe a peak in m'' most likely because m'' is typically two orders smaller than m'[3] and is below the detection limit of our instrument. One may wonder whether the signal from the AFM Cr$_2$O$_3$ layer may dominate the feature because the thickness of the Cr$_2$O$_3$ layer (30 nm) is more than 100 times higher than that of the Co layer (0.25 nm). We confirmed that no signal was detected for the Pt/Cr$_2$O$_3$ (130 nm)/Pt film where the Cr$_2$O$_3$ thickness is more than four times higher than the main film; and this is very reasonable considering the very low magnetic susceptibility of AFM materials and the small volume of the thin film. Moreover, as shown in Fig. 4 and Sec. III B, nonlinear MOKE loops were observed above the peak temperature, indicating that the Curie temperature of the ultrathin Co layer was higher than the peak temperature. These results indicate that the peak of the AC magnetization was caused by superparamagnetic blocking of the Co layer, that is, $T_{B\_SPM} = 283$ K.

In a typical superparamagnet, the peak temperature of the AC magnetization corresponding to T_{B_SPM} depends on the measurement frequency (f) through the relationship $f = f_0 \exp(\Delta E / k_B T_{B\_SPM})$,[3] where f_0 is a pre-factor ($\approx 10^9$ Hz), ΔE is the energy barrier for magnetization reversal, and k_B is the
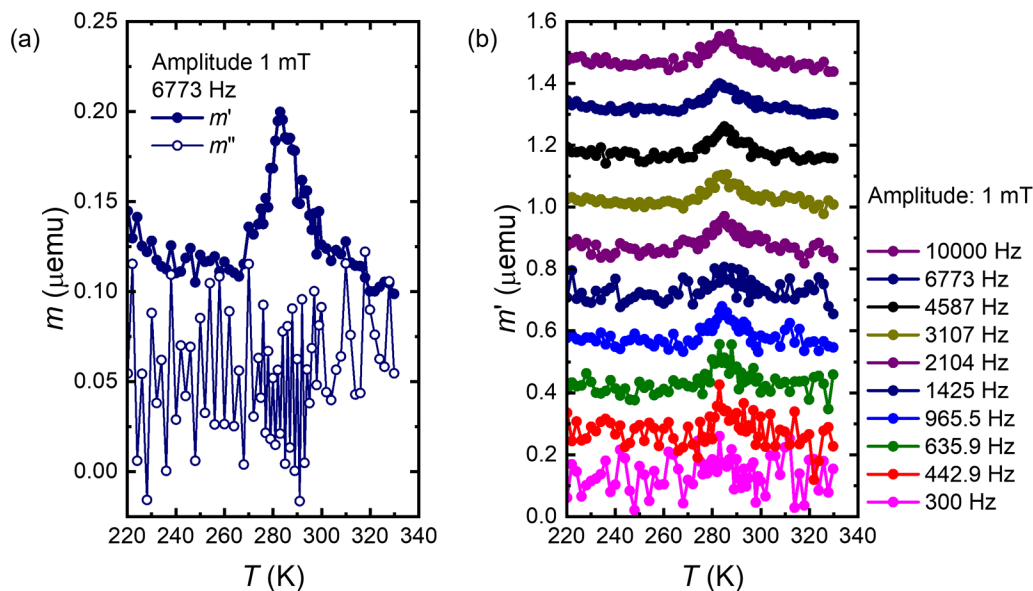
FIG. 3. Temperature dependence of AC magnetization. (a) Solid and open points represent the in-phase (real part) and off-phase (imaginary part) components of the reciprocal magnetization, respectively. Frequency of the excited AC field is 6773 Hz. (b) Series of the in-phase AC magnetizations measured at various frequencies. The points are shifted in the vertical direction for easier visibility.

Boltzmann constant. In Fig. 3(b), the temperature dependence of m' measured at various f values is shown. Although the peak at 300 Hz is difficult to observe owing to the low S/N ratio, the peaks above 442.9 Hz are observed. The peak temperature was almost constant for every f up to 10 kHz. The f-independent peak temperature implies that superparamagnetic blocking was dominated by the AFM ordering of the underlying AFM Cr_2O_3 layer.

At the end of this section, we briefly discuss the superparamagnetic features of the Co layer. In Fig. 4, the P-MOKE loop measured at 370 K is shown. It was difficult to capture the saturation region of the MOKE signal, and $\mu_0 H_C$ was almost zero. The experimentally obtained loop was fitted using the Langevin function (red curve). The magnetization per particle ($M_S V$) (2.2×10^{-20} J/T at 370 K) was used for fitting. Assuming the magnetic moment of Co to be 1.71 μ_B/Co (where μ_B is the Bohr magneton)[24] and the Wigner–Seitz cell radius of Co $\approx$ 2.6 a_B[25] (where a_B is the Bohr radius), the average diameter of Co is approximately 3 nm. Although there is no direct information on the microstructure of the ultrathin Co layer currently, ultrathin Co can form an island structure on Au,[26] and its estimated size is reasonably small to show superparamagnetism. Details of the microstructure of the Co layer are beyond the scope of this study and will be investigated in detail in the future.

B. Determination of T_{B_EB} and T_N

A series of P-MOKE loops measured at various temperatures are shown in Fig. 5(a). The temperature dependences of $\mu_0 H_{EB}$ and $\mu_0 H_C$ are summarized in Fig. 5(b). At 265 K, the hysteresis showed a sharp magnetization reversal, indicating that the film was in the
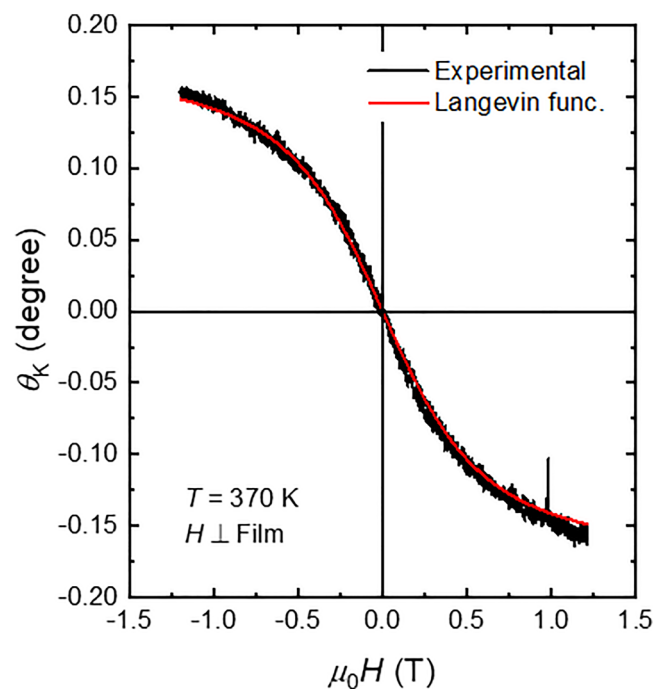

FIG. 4. P-MOKE loop measured at 370 K. Black and red lines represent the experimental data and the results calculated using the Langevin function, respectively.
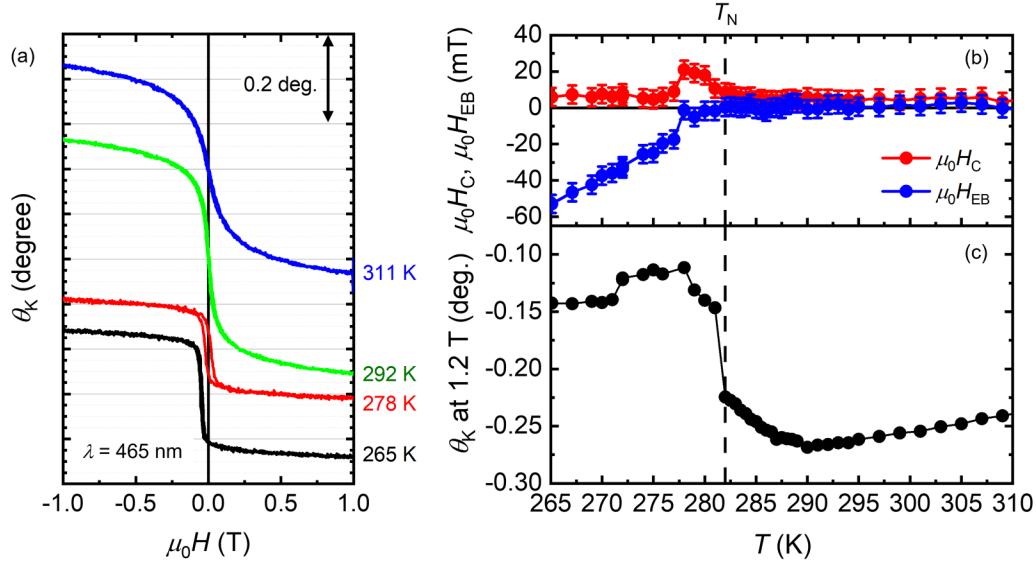
FIG. 5. (a) Examples of P-MOKE loops measured at various temperatures. Measurement temperatures were 265 (black), 278 (red), 292 (green), and 311 K (blue). The curves are shifted in the vertical direction for easier visibility. (b) Temperature dependence of exchange bias field $\mu_0 H_{EB}$ (blue) and coercivity $\mu_0 H_C$ (red). (c) Temperature dependence of polar Kerr rotation angle, θ_K, at $\mu_0 H = 1.2$ T. λ used for the measurement was 465 nm.

FM state. $\mu_0 H_{EB}$ was -53 mT at 265 K, decreased with increasing temperature, and became zero at 278 K, that is, $T_{B\_EB} = 278$ K. H_C formed a peak, which was accompanied by the disappearance of H_{EB}. After forming the peak, $\mu_0 H_C$ gradually decreased with increasing temperature and became almost zero above 284 K, which is very close to the peak temperature of AC magnetization. The slight difference in temperature is most likely because the two measurements were carried out using different instruments.

Interestingly, according to Fig. 5(a), the θ_K value also depends on the temperature. The temperature dependence of θ_K is shown in Fig. 5(c). The absolute value of θ_K ($|\theta_K|$) was approximately 0.10°–0.15° below 282 K, and it increased abruptly to 0.22° at 282 K. Upon further increasing the temperature, $|\theta_K|$ gradually increased to 0.27° and started to decrease again above 290 K. The gradual decrease in $|\theta_K|$ above 290 K was due to the superparamagnetism discussed in Sec. III A. Here, we discuss the abrupt change in θ_K at 282 K in association with the AFM ordering. In our film, the FM layer was grown on a transparent Cr_2O_3/Pt layer. In such a stacking structure, the intrinsic θ_K of the FM layer is modulated by optical interference in the transparent layer. This effect has been widely used to enhance the apparent θ_K in magneto-optic media.[27] As details on the optical interference effect on θ_K are given in the Appendix, θ_K is calculated using[28]

$$\theta_K = \text{Re}\left[\frac{E_{xy}}{\hat{N}(1-\hat{N}^2)}\right],$$

$$E_{xy} = \frac{\hat{N}_{tot}^{+2} - \hat{N}_{tot}^{-2}}{2i}, \quad \hat{N} = \frac{\hat{N}_{tot}^{+} + \hat{N}_{tot}^{-}}{2}, \tag{1}$$

where $\widehat{N_{tot}^{\pm}}$ denotes the effective refraction index of the entire film, considering the reflection at every interface. The superscript $\pm$ denotes the values for the right and left circularly polarized light. $\widehat{N_{tot}^{\pm}}$ includes the refractive index (n), extinction coefficient (k), and thickness (t) of each layer in the form of $\exp\left\{-i\frac{2\pi(n+ik)t}{\lambda}\right\}$. Because the optical interference, that is, the change in $\widehat{N_{tot}^{\pm}}$ with λ mainly causes in the transparent layer (the Cr_2O_3 layer), the apparent θ_K varies with n, k, and/or t of the Cr_2O_3 layer. These parameters usually exhibit a gradual temperature dependence, except for the structural phase transition[29] or magnetic ordering.[30] Although no structural phase transition has been reported for Cr_2O_3 in this temperature regime, the lattice parameters show a jump at T_N,[31] which leads to a change in θ_K via t at T_N. A change in the optical parameters accompanied by AFM ordering has also been observed in some antiferromagnets such as bulk MnO[30] and Cr_2O_3.[32] In the case of MnO, the temperature dependence of n exhibits an anomaly at T_N, which can be caused by a change in the magnetostrictive contribution at T_N.[30] In the case of Cr_2O_3, the dielectric tensor ϵ_{ij} of Cr_2O_3 depends on the AFM ordering parameter and its z component below T_N,[32] which supports that AFM ordering can change n and k [see Eq. (A2) in the Appendix]. In either case, the abrupt change in the apparent θ_K should be relevant to the AFM ordering; and T_N was determined to be 282 K. Notably, in Fig. 5(b), $\mu_0 H_C$ shows a tail above 282 K. This may be owing to the short-range ordering near the interface because of the stronger interfacial exchange coupling between Co and interfacial Cr^{3+} than that between Cr^{3+} ions at the bulk site.[33] This may also be owing to the finite time constant of the feedback system of the MOKE detection.

TABLE I. Summary of T_{B_SPM}, T_{B_EB}, and T_N. Measurement techniques are also shown in the right column.

Parameters	Estimated values (K)	Measurement technique
T_{B_SPM}	283	AC magnetization
T_{B_EB}	278	P-MOKE
T_N	282	P-MOKE

## C. Comparison of T_{B_SPM}, T_{B_SPM}, and T_N

Based on the above results, we determined that $T_{B\_SPM} = 283$ K from AC magnetization, $T_{B\_EB} = 278$ K, and $T_N = 282$ K from MOKE measurements, as summarized in Table I. Because T_{B_EB} and T_N were determined by the same measurements (Fig. 5), the temperature lag between these two is apparent. On the contrary, T_{B_SPM} and T_N are very similar to each other and are also similar to the T_N of the 20-nm-thick Cr_2O_3 thin film obtained by the spin Hall magnetoresistance measurements.[34] Namely, the relationship $T_{B\_EB} < T_{B\_SPM} \sim T_N$ is obtained. Notably, the relationship of $T_{B\_EB} < T_{B\_SPM}$ has been observed in other systems such as Co/IrMn,[35] Co/Pd multilayer/CoO,[36] and Au/Co/thermally oxidized Cr_2O_3,[37] in addition to the above-mentioned Co_{core}–CoO_{shell} NP system.[10]

Based on the above results, three temperature regimes were considered. The expected magnetic state in each regime is shown schematically in Fig. 6. At the temperature above T_N (temperature regime I), the AFM layer became paramagnetic, and the exchange anisotropy did not contribute to K_{eff}. Consequently, the Co layer transformed into the superparamagnetic state, where the remanent magnetization and coercivity are zero. At temperature slightly below T_N (temperature regime II), the interfacial exchange coupling enhanced the effective magnetic volume, and the magnetization of the Co layer was stabilized, resulting in finite coercivity; and hence, superparamagnetism was suppressed. In this temperature regime, the magnetic anisotropy energy of the AFM layer was still weak, and the AFM moments were reversed together with by FM magnetization reversal. Hence, a coercivity enhancement was observed instead of an exchange bias. In this way, T_N and T_{B_SPM} can match each other. Decreasing the temperature further below 278 K (temperature regime III), the regained magnetic anisotropy energy of the AFM layer pinned the AFM moments (or the Néel vector) against the FM magnetization reversal, for example, by forming a domain-wall-like structure in the AFM layer, which yields an exchange bias.[38,39]

IV. SUMMARY

We investigated the blocking temperatures for superparamagnetism and the exchange bias (T_{B_SPM} and T_{B_EB}, respectively) in association with the AFM ordering temperature, T_N. T_{B_SPM} was almost the same as T_N. Below this temperature, the interfacial
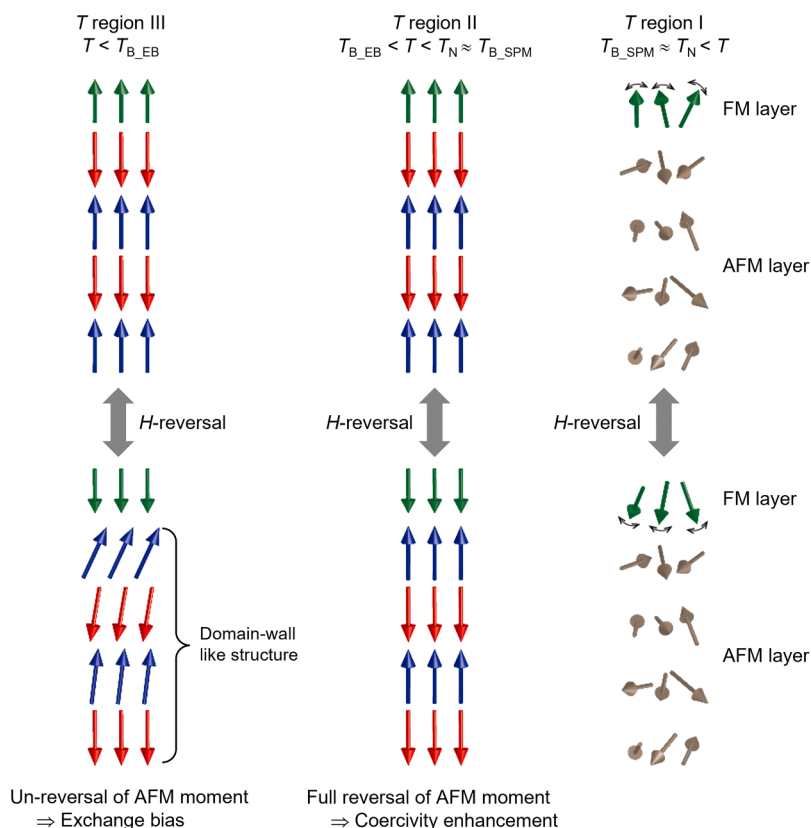
FIG. 6. Schematic drawings of the magnetic states at positive and negative magnetic fields. Green arrows represent the FM moments, and red and blue arrows represent AFM moments with two sublattices. Brown arrows represent the AFM moment at temperatures above T_N, i.e., the paramagnetic moment. In the schematic, the AFM interfacial coupling at the FM/Cr_2O_3(0001) and the canted spin alignment in the AFM layer near the interface in the temperature regime III are assumed.[38]
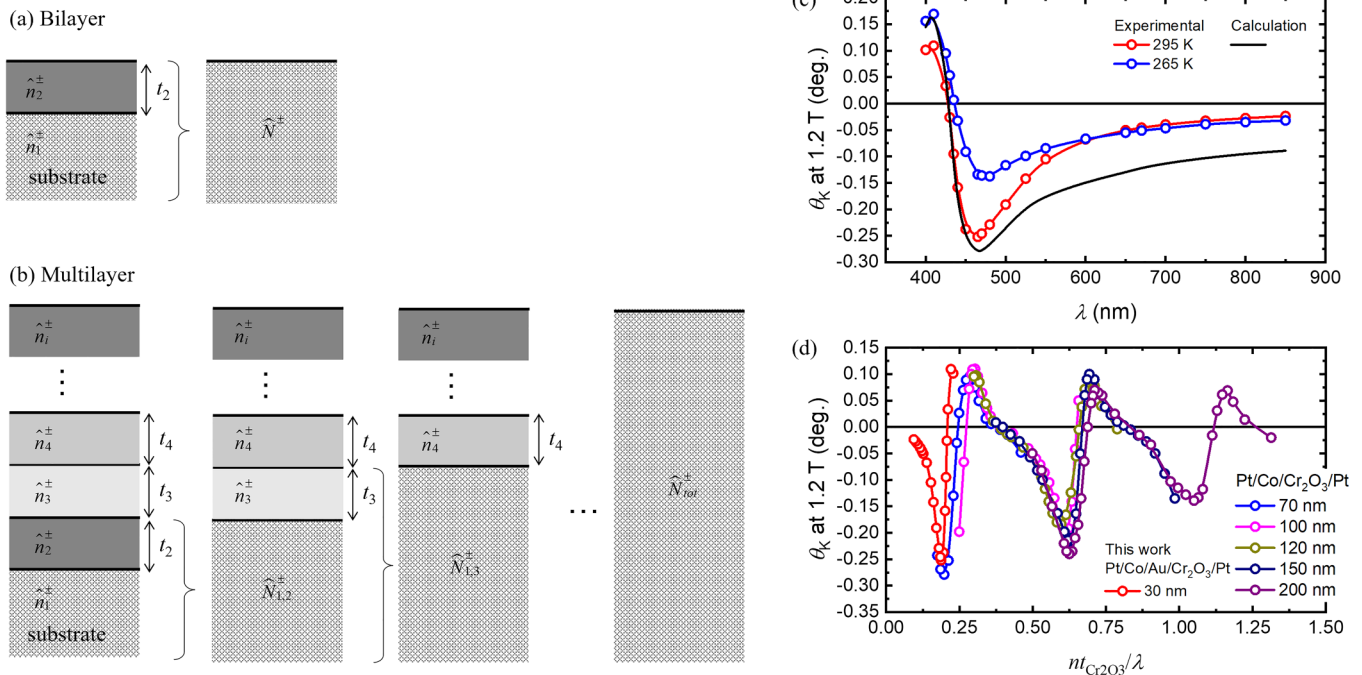
FIG. 7. Schematic of virtual optical constant model for (a) bilayer and (b) multilayer arrangements. (c) Example calculation with the experimentally obtained MOKE spectra. Red and blue symbols represent the results measured at 295 and 265 K, respectively, and black line represents the calculated result. (d) Reduced MOKE spectra, $\theta_K - n \cdot t_{Cr_2O_3}/\lambda$ curve for the various film with different $t_{Cr_2O_3}$.

exchange coupling at the FM/AFM interface increased the effective magnetic volume, which suppressed superparamagnetism. Upon further decreasing the temperature, the exchange bias appeared below 278 K, which is approximately 4 K lower than T_N ($\sim T_{B\_SPM}$). For the appearance of the exchange bias, the AFM moments must also be blocked against thermal agitation and FM magnetization reversal. Under these conditions, the magnetic anisotropy energy of the AFM layer must be higher than that for the criteria of superparamagnetic blocking, which is the reason for the temperature lag between T_N ($\sim T_{B\_SPM}$) and T_{B_EB}.

ACKNOWLEDGMENTS

AUTHOR DECLARATIONS

Conflict of Interest

The authors have no conflict to disclose.

DATA AVAILABILITY

The data that support the findings of this study are available from the corresponding author upon reasonable request.

APPENDIX: OPTICAL INTERFERENCE ON MAGNETO-OPTIC KERR ROTATION ANGLE IN THE STACKED FILM

The magneto-optic signal is described by the complex refractive index $\hat{N}^{\pm}$ ($= n^{\pm} - ik^{\pm}$), where the $\pm$ sign denotes the right and left circular polarizations of the light. For non-magnetic materials, that is, Pt buffer layer, Cr_2O_3 layer, Au layer, and Pt capping layer, $\hat{n}^{+} = \hat{n}^{-}$; and however, for a magnetic layer, that is, Co layer, $\hat{n}^{+} \neq \hat{n}^{-}$, which leads to the magneto-optic effect through[40]

$$\Phi_K = \frac{E_{xy}}{\hat{N}(1-\hat{N}^2)},$$

$$E_{xy} = \frac{\hat{n}^{+2} - \hat{n}^{-2}}{2i}, \quad \hat{N} = \frac{\hat{n}^{+} + \hat{n}^{-}}{2}, \tag{A1}$$

where Φ_K denotes the complex Kerr effect and θ_K is obtained from the real part of Φ_K.

In the thin-film system, the complex refractive index, $\hat{N}_2^{\pm}$ ($= n_2^{\pm} - ik_2^{\pm}$), of a layer with thickness t_2 on a substrate with $\hat{N}_1^{\pm}$ ($= n_1^{\pm} - ik_1^{\pm}$) is replaced by the virtual optical constant, $\hat{N}^{\pm}$, as shown in Fig. 7(a),
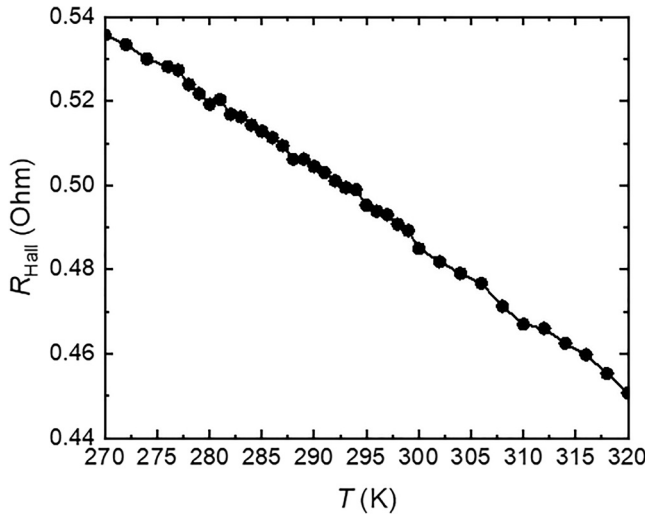
FIG. 8. Temperature dependence of anomalous Hall resistivity at $\mu_0 H = 2$ T.

$$\hat{N}^\pm = \hat{N}_1^\pm \frac{1 - r^\pm \exp(-2i\phi^\pm)}{1 + r^\pm \exp(-2i\phi^\pm)},$$

$$r^\pm = \frac{\hat{N}_2^\pm - \hat{N}_1^\pm}{\hat{N}_2^\pm + \hat{N}_1^\pm}, \quad \phi^\pm = \frac{2\pi \hat{N}_2^\pm t_2}{\lambda}, \quad \text{(A2)}$$

$$\hat{N}_j^\pm = \sqrt{\varepsilon_{xx\_j} \pm i\varepsilon_{xy\_j}}.$$

For the multilayer, this treatment was repeated, and a virtual index of the entire film, $\hat{N}_{tot}^\pm$, was evaluated [see Fig. 7(b)]. The apparent θ_K can be obtained by replacing $\hat{N}^\pm$ with $\hat{N}_{tot}^\pm$ in Eq. (A1). The experimentally obtained MOKE spectrum can be reproduced by the above model with suitable parameters. As an example, the MOKE spectra measured at 295 and 265 K, as well as the calculated spectrum, are shown in Fig. 7(c). With increasing λ, θ_K increased up to $\lambda \sim 420$ nm, sharply decreased, and reached a minimum at $\lambda = 465$ nm and increased gradually again. It can also be confirmed that θ_K at $\lambda = 465$ nm showed a large change for 297 and 265 K. Although the $\hat{N}_{Cr2O3}$-dependence of θ_K does not appear in the analytical form in Eqs. (A1) and (A2), comparing the obtained MOKE spectrum with the films with different t_{Cr2O3}, the MOKE spectra for the different t_{Cr2O3} could be scaled using $n \cdot t_{Cr2O3}/\lambda$ [Fig. 7(d)]. This is understood to be the phase of the reflected light changing as a function of $n \cdot t_{Cr2O3}/\lambda$.

One may still wonder whether the MOKE signal would be observed for the Cr_2O_3 layer alone and/or that the above spectrum might be affected by the bandgap of the Cr_2O_3 layer. We confirmed that no MOKE signal was obtained for Pt (2 nm)/Cr_2O_3 (30 nm)/Pt (20 nm). Moreover, the bandgap of Cr_2O_3 is reported to be above 3 eV,[41] which is higher than the photon energy for $\lambda = 465$ nm.

We further verified that the abrupt change in θ_K, as shown in Fig. 5(c), is caused by optical interference based on the AHE measurements. The MOKE signal originates from the off diagonal components of the dielectric tensor ϵ_{xy}, as shown in Eqs. (A1) and (A2), respectively. ϵ_{xy} can be converted into the conductivity tensor σ_{xy}. Because σ_{xy} causes the AHE, if the observed peculiarity of θ_K is caused by the inherent effect of the FM layer, a similar peculiarity would also appear in the temperature dependence of the AHE resistance (R_{AHE}). Figure 8 shows the temperature dependence of the R_{AHE} at $\mu_0 H = 2$ T. As can be seen, the R_{AHE} monotonically decreases with increasing temperature without any peculiarity, which supports the idea that the anomaly in θ_K is not caused by the inherent effect of the FM layer.

REFERENCES

[1]V. L. Pokrovsky, J. Magn. Magn. Mater. **200**, 515 (1999).

[2]Y. Shiratsuchi, M. Yamamoto, and S. D. Bader, Prog. Surf. Sci. **82**, 121 (2007).

[3]J. L. Dormann, D. Fiorani, and E. Tronc, *Magnetic Relaxation in Fine-Particle Systems*, Advances in Chemical Physics series, edited by I. Prigogine and S.A. Rice (Wiley, 1997), Vol. 98, pp. 283–494.

[4]R. H. Kodama, J. Magn. Magn. Mater. **200**, 359 (1999).

[5]Y. Shiratsuchi and M. Yamamoto, Phys. Rev. B **76**, 144432 (2007).

[6]H. Chen, Y. Yu, Z. Wang, Y. Bai, H. Lin, X. Li, H. Liu, T. Miao, Y. Kou, Y. Zhang, Y. Li, J. Tang, Z. Wang, P. Cai, Y. Zhu, Z. Cheng, X. Zhong, W. Wang, X. Gao, L. Yin, R. Wu, and J. Shen, Phys. Rev. B **99**, 214419 (2019).

[7]T. Ono, T. Moriya, M. Hatayama, K. Tsumura, N. Kikuchi, S. Okamoto, O. Kitakami, and T. Shimatsu, Appl. Phys. Lett. **110**, 022402 (2017).

[8]J. Wang, D. Liu, I. Suzuki, Y. Takahashi, M. Yan, and K. Hono, Appl. Phys. Express **12**, 023007 (2019).

[9]Y. Kamata, A. KiKitsu, N. Kihara, S. Morita, K. Kimura, and H. Izumi, IEEE Trans. Magn. **47**, 51 (2011).

[10]V. Skumyrev, S. Stoyanov, Y. Zhang, G. Hadjiyanayis, D. Givord, and J. Nogués, Nature **423**, 850 (2003).

[11]T. Nozaki, M. Oida, T. Ashida, N. Shimomura, and M. Sahashi, Appl. Phys. Lett. **103**, 242418 (2013).

[12]C. Wang, C. Xu, M. Wang, Y. Yuan, H. Liu, L. Dillemans, P. Homm, M. Menghini, J.-P. Locquet, C. Van Haesendonck, S. Zhou, S. Ruan, and Y.-J. Zeng, J. Phys. D: Appl. Phys. **50**, 495002 (2017).

[13]J. de la Venta, S. Wang, T. Sarbeck, J. G. Ramírez, I. Valmianski, and I. K. Shuller, Appl. Phys. Lett. **104**, 062410 (2014).

[14]J. Nogués and I. K. Schuller, J. Magn. Magn. Mater. **192**, 203 (1999).

[15]P. Borisov and W. Kleemann, J. Appl. Phys. **110**, 033917 (2011).

[16]S. Pati, N. Shimomura, T. Nozaki, T. Shibata, and M. Sahashi, J. Appl. Phys. **117**, 17D137 (2015).

[17]P. Borisov, A. Hochstrat, X. Chen, W. Kleemann, and C. Binek, Phys. Rev. Lett. **94**, 117203 (2005).

[18]Y. Shiratsuchi, K. Toyoki, and R. Nakatani, J. Phys. Condens. Matter. **33**, 243001 (2021).

[19]Y. Shiratsuchi, H. Oikawa, S. Kawahara, Y. Takechi, T. Fujita, and R. Nakatani, Appl. Phys. Express **5**, 043004 (2012).

[20]Y. Shiratsuchi, T. Fujita, H. Noutomi, H. Oikawa, and R. Nakatani, IEEE Trans. Magn. **47**, 3909 (2011).

[21]Y. Shiratsuchi, W. Kuroda, T. V. A. Nguyen, Y. Kotani, K. Toyoki, T. Nakamura, M. Suzuki, K. Nakamura, and R. Nakatani, J. Appl. Phys. **121**, 073902 (2017).

[22]Y. Shiratsuchi, Y. Tao, K. Toyoki, and R. Nakatani, Magnetochemistry **7**, 36 (2021).

[23]L. M. Corliss, J. M. Hastings, R. Nathans, and G. Shirane, J. Appl. Phys. **36**, 1099 (1965).

[24]R. M. Bozorth, *Ferromagnetism* (John Wiley and Sons, Inc., 2003), p. 264.

[25]A. L. Kutepov, J. Phys. Condens. Matter. **29**, 465503 (2017).

[26]N. Weiss, T. Cren, M. Epple, S. Rusponi, G. Baudot, S. Rohart, A. Tejeda, V. Repain, S. Rousset, P. Ohresser, F. Scheurer, P. Benock, and H. Brune, Phys. Rev. Lett. **95**, 157204 (2005).

[27]Y. Wang, W. M. Zheng, S. M. Zhou, L. Y. Chen, W. R. Zhu, D. L. Qian, Y. X. Zheng, H. Y. Zhang, and J. Huang, J. Appl. Phys. **81**, 1956 (1997).

[28]K. Sato, H. Kida, and T. Katayama, Jpn. J. Appl. Phys. **27**, L237 (1988).

[29]P. A. Santoro, A. R. Sampaio, H. L. F. da Luz, and A. P. Palangana, Phys. Lett. **353**, 512 (2006).

[30]T. Moriyasu, S. Wakabayashi, and T. Kohmoto, J. Infrared Millim. Terahertz Waves **34**, 277 (2013).

[31]H. L. Alberts and J. C. A. Boeyens, J. Magn. Magn. Mater. **2**, 327 (1976).

[32]R. V. Pisarev, B. B. Krichevtsov, and V. V. Pavlov, Phase Transitions **37**, 63 (1991).

[33]R. Choudhary, T. Komesu, P. J. Kumar, P. Manchanda, K. Taguchi, T. Okuda, K. Miyamoto, P. A. Dowben, R. Skomski, and A. Kashyap, Europhys. Lett. **115**, 17003 (2016).

[34]T. Iino, T. Moriyama, H. Iwaki, H. Aono, Y. Shiratsuchi, and T. Ono, Appl. Phys. Lett. **114**, 022402 (2019).

[35]H. Kanso, R. Patte, and D. Ledue, J. Magn. Magn. Mater. **491**, 165543 (2019).

[36]M. Perzanowski, M. Marszalek, A. Zarzycki, M. Krupinski, A. Dziedzic, and Y. Zabila, ACS Appl. Mater. Interfaces **8**, 28159 (2016).

[37]Y. Shiratsuchi, T. Nakatani, S. Kawahara, and R. Nakatani, J. Appl. Phys. **106**, 033903 (2009).

[38]Y. Shiratsuchi, H. Noutomi, H. Oikawa, T. Nakamura, M. Suzuki, T. Fujita, K. Arakawa, Y. Takechi, H. Mori, T. Kinoshita, M. Yamamoto, and R. Nakatani, Phys. Rev. Lett. **109**, 077202 (2012).

[39]C. Mitsumata, M. Tsunoda, H. Takahashi, and A. Sakuma, Europhys. Lett. **99**, 47006 (2012).

[40]R. Fang, C. Peng, T. Ma, P. Long, J. Liu, Y. Nin, and D. Dai, J. Appl. Phys. **74**, 6830 (1993).

[41]A. Rohrbach, J. Hafner, and G. Kresse, Phys. Rev. B **70**, 125426 (2004).